Ba $6p_j nf_{j'}$ autoionizing series

R. R. Jones, C. J. Dai, and T. F. Gallagher
Department of Physics, University of Virginia, Charlottesville, Virginia 22901
(Received 5 September 1989)

Members of the $6p_j nf_{j'}$ autoionizing series in barium have been observed experimentally using multistep laser excitation. The recorded spectra exhibit extremely broad profiles for n values ranging from 7 to 30. We have fitted the spectra using an energy-independent multichannel quantum-defect theory model that reproduces the data reasonably well in spite of the fact that the full widths at half maximum of the excitation profiles are comparable in magnitude to the energy spacings between adjacent states. Experimental quantum defects and autoionization rates are presented along with the parameters determined from the theoretical fit.

I. INTRODUCTION

Over a decade ago the isolated core excitation (ICE) technique was developed in order to study autoionizing states in alkaline-earth-metal atoms.[1] In most cases this method yields spectra that are characteristic of the autoionizing series of interest only, with no dependence on the underlying continua. The technique simplifies data analysis greatly by suppressing the interference effects due to excitation of the degenerate continua, making it particularly easy to determine the useful parameters of a particular autoionizing series (namely the quantum defects and autoionization rates). In many cases multichannel quantum defect theory (MQDT) has been used to reduce the data, and to date the theory has enjoyed great success, particularly in the study of Ba $6pnl$ states and Sr $5pnl$ levels.[2-5]

Here we report the use of a combined laser excitation and radiative decay scheme in an ICE of Ba $6p_j nf(p)$ autoionizing states. In particular, we have studied the $6p_j nf_{j'}$ $J=4$ levels in detail, collected spectra for $n=7-30$, and fitted the data using a six-channel MQDT model. Experimentally, the excitation profiles exhibit extremely broad features and strong interactions between series converging to the Ba^+ $6p_{1/2}$ and $6p_{3/2}$ limits. The observed full widths at half maximum (FWHM) of the profiles are approximately one-third of the energy spacings between adjacent levels of a given series. To our knowledge these are the broadest levels ever studied using the ICE approach. In fact, in this case ICE loses some of its comparative advantage in unmasking the interesting parameters of the autoionizing series.

In the following sections we discuss our experimental procedure and results. We then present the theoretical model used for our analysis along with the set of MQDT parameters which best reproduce the observed spectra. We also discuss the applicability of the ICE approach to describing extremely broad autoionizing levels. We conclude with a review of studies of Ba $6pnl$ autoionizing states and a brief discussion of the gross features of the variation of autoionization rates with l.

II. EXPERIMENTAL PROCEDURE

The laser excitation scheme and apparatus we use has been described in detail in other works.[1,3] Therefore the description here will be brief and will highlight only the new aspects in the procedure. As shown in Fig. 1, three pulsed, tunable dye lasers are used to excite Ba atoms to the $6p_j nf(p)$ states of interest. The first dye laser excites the Ba $6s6p\ ^1P_1$ state from the ground state. This level decays within a few nanoseconds to the $6s^2$ ground state or to a $6s5d$ metastable level. The branching ratio for decay to the metastable state is less than 5%.[4] 50 ns after the first laser the atoms are excited to a $6snf(p)$ Rydberg

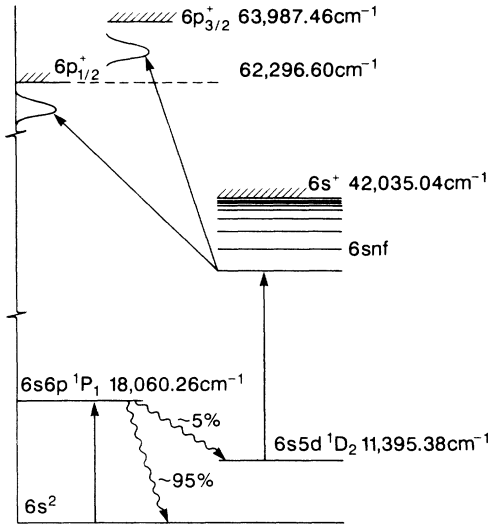

FIG. 1. Schematic of the laser excitation scheme. A single photon excites the Ba $6s6p\ ^1P_1$ resonance line which decays to the $6s^2$ ground state or to a $6s5d\ ^1D_2$ metastable state. A second dye laser then excites a $6snf$ Rydberg level from the metastable state. The final excitation is provided by a third dye laser which drives the Ba^+ $6s$-$6p_j$ transition, thus creating a $6p_j nf$ autoionizing state.

state from the $6s5d\ ^1D_2$ metastable level by the frequency doubled output of a second laser with a wavelength of $\simeq 680$ nm. The final step of the excitation is accomplished using the third dye laser and is the isolated Ba^+ core $6s_{1/2}$-$6p_j$ transition. The first dye laser is a commercial laser and is pumped using a XeCl excimer laser. The second and third lasers are of the Hansch[6] type and are pumped by the second and third harmonics of an Nd:YAG (where YAG is yttrium aluminum garnet) laser, respectively. All three dye lasers have pulse energies of $\simeq 100\ \mu J$, have pulse widths of 10 ns, and are pulsed at a 20-Hz repetition rate. All three lasers are linearly polarized in the same direction or circularly polarized in the same sense for different final-state angular momentum selections.

The laser beams interact with an effusive beam of Ba atoms in a vacuum chamber with a background pressure of 10^{-7} Torr. The three lasers enter the chamber colinearly and at a right angle to the atomic beam. Ba atoms are excited in a small region between two 8×8 cm^2 aluminum field plates which are separated by a distance of 2.5 cm. After the atoms autoionize, a small voltage ($\simeq 100$ V) is applied to the lower plate, which pushes the Ba^+ ions toward a dual microchannel plate detector, which is located nearly 10 cm above the upper field plate.

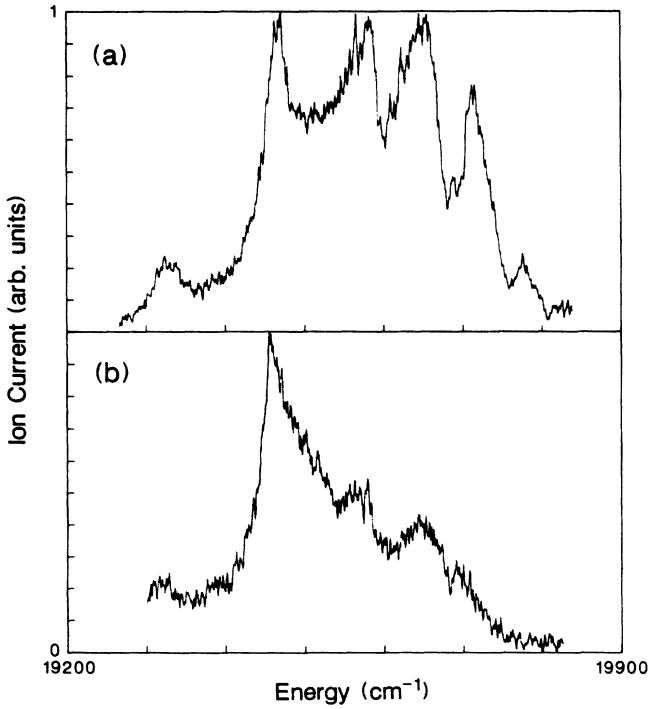

FIG. 2. Frequency scans of the third dye laser over the $6p_{3/2}7f$ autoionizing state. (a) Excitation profile obtained when all three lasers are vertically polarized. (b) Profile obtained with all three lasers circularly polarized in the same sense. Note the obvious suppression of final states with $J\neq 4$ for circularly polarized light and the interference in the broad feature due to the degenerate $6p_{1/2}nf$ series ($n\simeq 12$). The energy scale is relative to the first ionization limit.

The ion current is then amplified, integrated in a boxcar averager, and digitized to be stored on a personal computer.

By fixing the frequency of the second laser we excite a particular $6snf(p)$ Rydberg level. Then, by scanning the frequency of the third laser over a frequency range around the Ba^+ $6s$-$6p_j$ energy interval, we observe the energy dependence of the $6snf(p)$-$6p_jnf(p)$ excitation cross section. The power of the third laser is kept at a level such that there is no depletion broadening[7] of the profile. Also, when the three lasers are linearly polarized, the first laser beam is reflected back through the interaction region before the other lasers are fired. This scheme allows us to double the population in the metastable $6s5d\ ^1D_2$ level, thus doubling the population in the final autoionizing state. Unfortunately, with circular polarization the reflected laser pulse would become circularly polarized in a sense opposite to that of the incident beam and would destroy the angular momentum selectivity of the circularly polarized beams. Therefore, when all three lasers are circularly polarized, the first laser is sent through the interaction region only once giving a reduced signal-to-noise ratio.

III. EXPERIMENTAL RESULTS

Scans of the third laser frequency were performed using both circularly and linearly polarized laser beams for excitation to $6p_{3/2}nf$ and $6p_{1/2}nf$ final states with n ranging from 7 to 30. The excitation profiles of the $6p_{1/2}nf$ levels using circularly polarized light are nearly identical to those obtained using linearly polarized light. These profiles are approximately Lorentzian and exhibit only one dominant feature. The $6p_{3/2}nf$ levels, on the other hand, have vastly different appearances when using circularly or linearly polarized light. Scans of the third laser frequency using circularly polarized light generate spectra that exhibit one or two broad overlapping resonances. Those scans taken with linear polarization often show three or more distinct peaks. Figures 2 and 3 clearly show the differences between the circular and linear polarization spectra for the highly perturbed $6p_{3/2}7f$ and $6p_{3/2}8f$ levels.

Of course, we expect to see different profiles using the two different polarizations due to the different angular momentum selection rules. Consider our excitation scheme assuming that the two intermediate states $6s5d\ ^1D_2$ and $6snf\ ^1F_3$, are well-defined singlet levels and that the final $6p_jnf_{j'}\ J$ autoionizing states are well defined as jj coupled levels. Furthermore, assume that the spontaneous decay to the $6s5d$ level is completely isotropic in M, the z projection of the total angular momentum of the outer two electrons. Using linearly polarized light to excite $6p_{1/2}nf_{j'}\ J$ levels should yield 40% of the total excitation in a $j'=\frac{5}{2}$, $J=2$ level and 55% in a $j'=\frac{7}{2}$, $J=4$ level. If we use circularly polarized light instead, we should find over 91% of the total excited population in a $j'=\frac{7}{2}$, $J=4$ level with approximately 8% split between $j'=\frac{5}{2}$ or $\frac{7}{2}$, $J=3$ states. Thus, when exciting the $6p_{1/2}nf$ states, we might expect to see two strong features using linearly polarized light and only one feature in the pres-

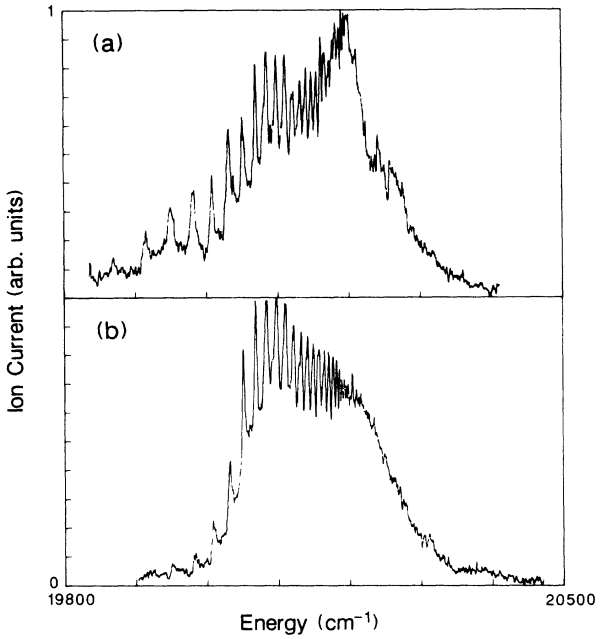

FIG. 3. Excitation profile of the $6p_{3/2}8f$ state analogous to Fig. 2 with vertical polarization in (a) and circular polarization in (b). The interference is again due to the degenerate $6p_{1/2}nf$ series. Note that the interference pattern gradually smooths away as the $6p_{1/2}nf$ series becomes a continuum above the $6p_{1/2}$ limit at 20261.56 cm^{-1} (Ref. 8). The energy scale is relative to the first ionization limit.

ence of circularly polarized light. However, the fact that we observe only one feature using linear polarization, which is identical to the one seen using circularly polarized light, suggests that the $j'=\frac{5}{2}$, $J=2$ state is degenerate with the $j'=\frac{7}{2}$, $J=4$ level. This situation has, in fact, been observed previously in the study of Ba $6png$ levels by Jaffe *et al.*[4]

Now consider the case of excitation to $6p_{3/2}nf_{j'}$ J levels using the same assumptions discussed above. For linearly polarized light we expect to see over 35% of the net excitation to $j'=\frac{7}{2}$, $J=2$ levels, 34% to $j'=\frac{5}{2}$, $J=4$ states, nearly 20% to $j'=\frac{7}{2}$, $J=4$ levels, and less than 8% to the $j'=\frac{5}{2}$, $J=2$ and 3 levels. The schematic simplifies drastically with circular polarization, with 57% of the excitation driving $j'=\frac{5}{2}$, $J=4$ levels and over 31% of the population residing in $j'=\frac{7}{2}$, $J=4$ states. None of the $J=2$ or 3 levels controls more than 5% of the total population. Thus, by using circular polarization, the excitation of the $6p_jnf_{j'}$ J levels is strongly dominated by three bound $J=4$ channels, $j=\frac{1}{2}$, $j'=\frac{7}{2}$; $j=\frac{3}{2}$, $j'=\frac{7}{2}$; and $j=\frac{3}{2}$, $j'=\frac{5}{2}$.

Due to the relative simplicity of the spectra, we shall confine our attention here to the $J=4$ levels reached using circularly polarized light. There is, however, another complication in our excitation scheme. The $6snf$ Rydberg series is not well described in LS coupling, particularly in the region between $n=9$ and 20 where the series is perturbed by $5d4f$ and $5d8p$ levels.[9] Since our second laser excitation is from a well-characterized singlet level, we should only be able to excite singlet character in the the $6snf$ Rydberg series. However, in many cases we observe comparable excitation strengths to two nf levels for a given n. Thus we believe that in these instances the $6snf$ series may be more properly described as a jj coupled series. Therefore, whenever it has been possible to excite both the red and blue states of the doublet for a given n, we have studied the autoionization spectra originating from both levels. The final states that are excited should be the same using either member of a $6snf$ Rydberg doublet as an initial state, but the relative amplitudes of the autoionizing channels will be different depending on the difference in the admixture of $nf_{5/2}$ and $nf_{7/2}$ character in the red and blue states.

The experimental widths and energy level positions of the observed $6p_jnf_{j'}$ $J=4$ states are reported in Table I for values of n from 7 to 30. The scaled autoionization rates ($n^3\Gamma$) are plotted in Fig. 4 and the quantum defects are plotted in Fig. 5. The values shown were obtained by fitting the data to a single Lorentzian for $j=\frac{1}{2}$ or the sum of two Lorentzians for $j=\frac{3}{2}$. This choice of line shape assumes that there is little or no interseries interaction. The number of Lorentzians for a given value of j was chosen according to the number of allowed levels from angular momentum selection rules. Since a Lorentzian profile is implicit in the assumption of an exponential autoionization decay, we feel that this type of fit is a reasonable method for presenting the "raw" experimental results. The values shown in Table I and plotted in Figs. 4 and 5 are the average values from at least two independent measurements for each state, and for $n=10-14$ and 16, the results from both red and blue $6snf$ initial states have been used. For n values greater than 19 the parameters shown were deduced by taking the observed positions and widths without numerical fitting. For these states the quantum defects between the initial and final states of the excitation differ by nearly one-half and thus the profiles exhibit nearly equal amplitudes to final states with principal quantum number n and $n+1$.[3] Fitting these profiles to single or double Lorentzians would have been meaningless and would have produced misleading results. Also, due to the $5d8d$ perturber near $n=20$ and the dye gain fall off, the signal-to-noise ratio of the data for $n>19$ is significantly smaller than for $n<19$. Therefore only a few experimental results are listed for $n>19$.

IV. THEORETICAL ANALYSIS

Background

Our theoretical analysis is based on the MQDT formalism of Cooke and Cromer[10] and assumes that our experimental method does, in fact, use a true isolated core excitation. First, we present the basic equations of our analysis before moving to the specific four-channel and six-channel models that were actually used to fit the data. As was mentioned previously, the $6snf$ Rydberg series is not well represented in LS coupling. Therefore we describe the initial $6snf$ state as a linear combination of

TABLE I. Experimental energy levels and profile widths (FWHM) for $6p_jnf_{j'}$ $J=4$ autoionizing states. The parameters reported here were determined by fitting the observed profiles to a single Lorentzian for $j=\frac{1}{2}$ and to the sum of two Lorentzians for $j=\frac{3}{2}$. Parameter values are also the average values obtained from several different scans using both members of the $6snf$ doublet as initial states. Energies are given relative to the ground state, and both the level positions and widths are in cm^{-1}.

n	$6p_{1/2}nf_{7/2}$		$6p_{3/2}nf_{5/2}$		$6p_{3/2}nf_{7/2}$	
	Energy	Width	Energy	Width	Energy	Width
7	59 968	184				
8	60 484	99	62 139	101	62 260	138
9	60 849	141	62 537	105	62 597	100
10	61 162	87	62 826	71	62 874	74
11	61 359	44	63 031	39	63 088	58
12	61 503	32	63 185	25	63 209	51
13	61 622	50	63 306	19	63 326	26
14	61 721	38	63 402	14	63 417	29
15	61 797	24	63 476	16	63 489	16
16	61 855	20	63 549	11	63 555	17
17	61 909	13	63 600	8	63 604	21
18	61 957	11	63 638	14	63 642	11
19	61 989	10	63 671	15	63 679	5
20						
21						
22	62 067	3.3				
23	62 087		63 777			
24						
25	62 118	2.8	63 809			
26	62 131		63 822			
27			63 834			
28			63 844			
29			63 853			
30			63 863			

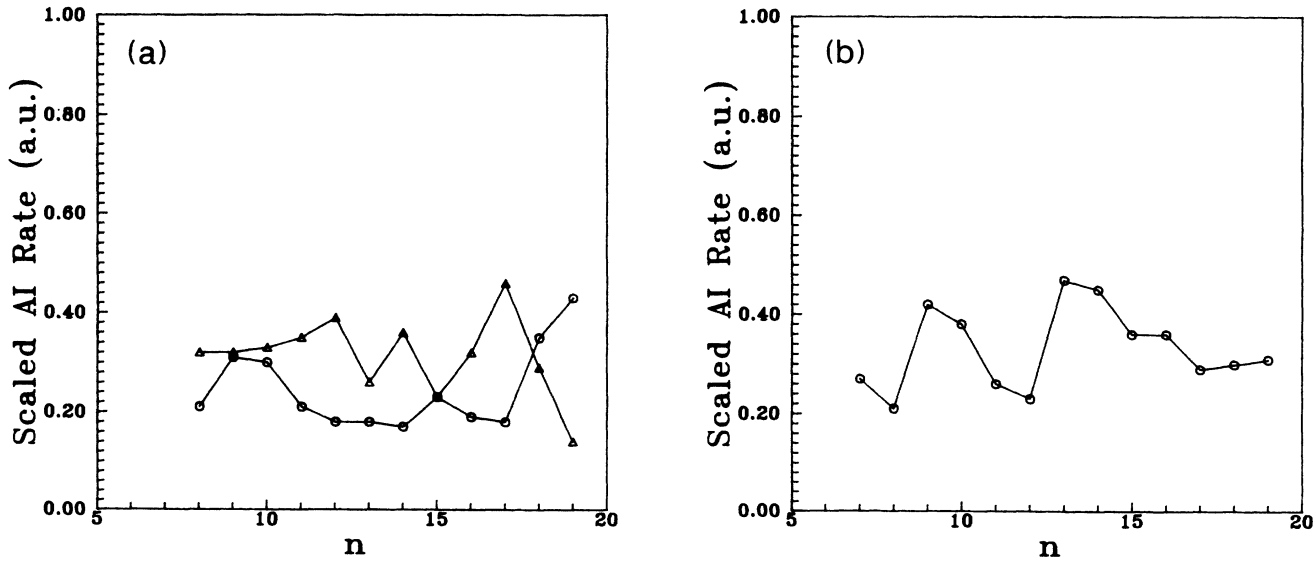

FIG. 4. Scaled autoionization rates $n^3\Gamma$ for the (a) $6p_{3/2}nf_{5/2}$ (○) and $6p_{3/2}nf_{7/2}$ (△) series and (b) $6p_{1/2}nf_{7/2}$ (○) levels as a function of principal quantum number n. The rates Γ are taken as the FWHM of the Lorentzian profiles which were fit to the data. All rates are given in atomic units.

$J=3$, jj coupled states. Thus the red state of a given n has the wave function

$$\Phi_r=\cos(\theta)|6s_{1/2}nf_{5/2}\rangle_{J=3}+\sin(\theta)|6s_{1/2}nf_{7/2}\rangle_{J=3}\ , \tag{1a}$$

and the blue state is represented as

$$\Phi_b=-\sin(\theta)|6s_{1/2}nf_{5/2}\rangle_{J=3}+\cos(\theta)|6s_{1/2}nf_{7/2}\rangle_{J=3}\ , \tag{1b}$$

where θ is a rotation angle which gives the admixture of $nf_{5/2}$ and $nf_{7/2}$ character in the initial state. Due to the large perturbations in the $6snf$ series mentioned previously, the value of θ is allowed to vary for each n but must have the same value for both states of the doublet for each n.

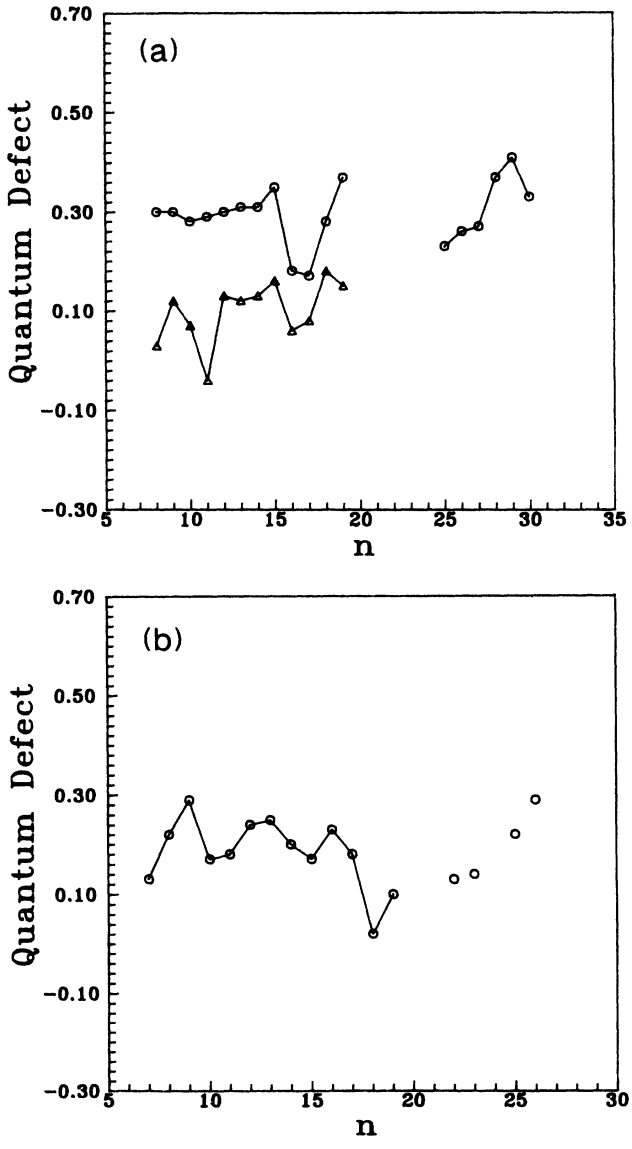

FIG. 5. Measured quantum defects for the (a) $6p_{3/2}nf_{5/2}$ (○) and $6p_{3/2}nf_{7/2}$ (△) series and (b) $6p_{1/2}nf_{7/2}$ (○) levels. The quantum defects were derived from the peak positions of the Lorentzian fits to the excitation profiles.

The final state of our excitation can be written as

$$\Psi=\sum_i A_i\psi_i\ ,$$

where

$$\psi_1=|6p_{3/2}nf_{5/2}\rangle_{J=4}\ , \tag{2a}$$

$$\psi_2=|6p_{3/2}nf_{7/2}\rangle_{J=4}\ , \tag{2b}$$

$$\psi_3=|6p_{1/2}nf_{7/2}\rangle_{J=4}\ , \tag{2c}$$

ψ_4, ψ_5, and ψ_6 represent the generalized continuum, and A_i is the energy-dependent spectral amplitude for a given channel. Note that Ψ contains both bound-state and continuum character. Thus the excitation amplitude to a final state Ψ from an initial bound state Φ consists of a sum of six terms, one for each of the six collision channels above. Fortunately, we can ignore the three terms which correspond to direct continuum excitation. Using ICE, direct population of the continuum is several orders of magnitude less probable than bound-state excitation. Thus we can neglect the presence of the underlying continua in our theoretical reproduction of the spectrum. The three bound channels used for the final-state wave function are the major contributors to the $6pnf$ profiles with circularly polarized laser light. The final-state wave functions used here are assumed to be energy normalized.

The excitation moment from the initial Rydberg state to a final autoionizing eigenchannel when using circularly polarized light can be written as

$$\mu=\frac{1}{\nu_i^{3/2}}\langle\Psi|rC_1^1|\Phi\rangle\ , \tag{3}$$

where C_1^1 is the spherical harmonic operator for circularly polarized light and the factor of $1/\nu_i^{3/2}$ is a normalization factor due to the fact that the initial Rydberg state wave function is normalized to 1. Consider a generic initial state $\Phi=|6s_{1/2}nl_{j'}\rangle$ and final state $\Psi=|6p_jnl'_{j'}\rangle$. Then in the ICE scheme Eq. (3) can be written as

$$\mu=\frac{1}{\nu_i^{3/2}}\langle 6p|r|6s\rangle\langle\nu_i l|\nu l'\rangle\chi A(\nu)\ , \tag{4}$$

where ν_i is the effective quantum number of the initial Rydberg state ($\nu_i=n_i-\delta_i$, where δ_i is the quantum defect of the initial state), ν is the effective quantum number corresponding to a given energy in the final-state spectrum, χ contains all angular and spin factors, and $A(\nu)$ is the energy-dependent spectral amplitude of Ψ. The overlap integral can be expressed in closed form to a very good approximation in atomic units as[11]

$$\langle\nu_i l|\nu l'\rangle=\delta_{l,l'}\frac{\sin[\pi(\nu_i-\nu)]}{\pi(W_i-W)}\ , \tag{5}$$

where W_i is the energy of the Rydberg level with respect to the first ionization limit and W is the energy of a position in the final-state spectrum with respect to the $6p_j$ ion limit.

Using Eqs. (4) and (5) we can write out the excitation moment from an initial red $6snf$ Rydberg state to a particular eigenchannel Ψ

$$\mu=\frac{1}{\nu_i^{3/2}}\mu_{6s\text{-}6p}[A_1\cos(\theta)\Omega_1\chi_1+A_2\sin(\theta)\Omega_2\chi_2 + A_3\sin(\theta)\Omega_3\chi_3] , \quad (6)$$

where $\mu_{6s\text{-}6p}$ is the radial part of $\langle 6p|r|6s\rangle$, the Ω_i refer to the overlap integrals from Eq. (5), and the subscripts i correspond to the components ψ_i in the eigenchannel Ψ. [The moment from an initial blue state has the same form and we only need to replace $\cos(\theta)$ by $-\sin(\theta)$ and $\sin(\theta)$ by $\cos(\theta)$.] The only factors left to determine are the amplitudes A_i of the collision channels ψ_i in the eigenchannels Ψ and it is to this end that the MQDT analysis has been used.

The MQDT equations we have used were first presented by Cooke and Cromer[10] and their choice of parameters is particularly useful in describing ICE spectra. The problem at hand is to determine the energy-dependent amplitudes of the bound and continuum collision channels in the correct basis set (i.e., in the eigenchannels). The basic equation to be solved is the pseudoeigenvalue problem

$$[\underline{R'}+\underline{\tan(\pi\nu')}]\mathbf{a'}=0 , \quad (7)$$

where the symmetric matrix $\underline{R'}$ has only off-diagonal elements which represent couplings between different channels (bound and continuum) and the matrix $\underline{\tan(\pi\nu')}$ is diagonal. The quantum number ν_j' is defined in terms of the effective quantum number of a given energy position and the quantum defect δ_j of the jth channel

$$\nu_j'=\nu_j+\delta_j .$$

The vector $\mathbf{a'}$ has components

$$a_i'=\cos(\pi\nu_i')A_i ,$$

where A_i is the amplitude of the ith collision channel in an eigenchannel.

Consider the case where there are n_b bound channels and n_c continuum channels. Following the procedure outlined by Cooke and Cromer[10] the matrix equation given by Eq. (7) can be reduced to an n_c-dimensional eigenvalue problem if no information about the absolute phase of the continuum waves is desired. Since our ion spectra yield no information on the absolute phases of the different continua, this approach is used to greatly simplify our problem. When this method is employed the continuum waves are used only to normalize the final wave function.

In reality there are many continuum paths available to an autoionizing $6pnf$ level, and all are present in the true wave function describing the atomic system below the $6p_{3/2}$ limit of the Ba^+ ion. However, it can be shown that the most general description of a system in the MQDT formalism can be obtained if we have $n_c=n_b$ continuum channels. This simplification is possible if we ignore the actual composition of the continua used in the fit. In our fit we choose a set of continua such that each continuum is coupled to only a single bound channel. This choice is a rotation of the actual continua which simplifies the calculations significantly by allowing us to set several of the $\underline{R'}$ matrix elements to zero. Unfortunately, by choosing this basis we throw away any information on the composition of the actual continua, i.e., the relative fractions of $6s\epsilon g$, $6s\epsilon p$, $5d\epsilon d$, etc.

Four-channel analysis above the Ba^+ $6p_{1/2}$ limit

In an attempt to simplify the analysis, the data has been analyzed separately for the energy regions above and below the Ba^+ $6p_{1/2}$ limit. Above the limit the system can be reasonably well described by a four-channel model [two bound channels, ψ_1 and ψ_2 from Eq. (2), and the two generalized continuum channels]. The parameters obtained from the fit of the levels above the limit can then be used directly in the analysis of states below the $6p_{1/2}$ limit. Because there are relatively few MQDT parameters to be determined in the four-channel fit (there are only six), we have also used the spectra above the limit to establish the proper values of the rotation angle θ for the Rydberg states. These values were obtained by treating θ as a free parameter in finding the best fit for the observed spectra of a given n. The spectrum we calculate is simply

$$\sigma=C\sum_i^{n_c}|\mu_i|^2 ,$$

where the μ_i are obtained from Eq. (6) with an arbitrary energy independent amplitude C for each initial state. (In using $\sum_i|\mu_i|^2$ as being proportional to the total cross section, we have ignored the small changes in the frequency of the third laser over the excitation profile.) Since we are using an arbitrary amplitude for each energy level, we need to put the ratio of the angular integrals χ into the fit. For the two bound channels used, this ratio has the value $\chi_2/\chi_1=\sqrt{5/12}$.

The set of MQDT parameters obtained from our fit are

$$\underline{R'}=\begin{vmatrix} 0 & -0.083 & 0.63 & 0 \\ -0.083 & 0 & 0 & 0.80 \\ 0.63 & 0 & 0 & -0.050 \\ 0 & 0.80 & -0.050 & 0 \end{vmatrix} ,$$

$$\delta_1=\delta_{6p_{3/2}nf_{5/2}}=0.31 ,$$

and

$$\delta_2=\delta_{6p_{3/2}nf_{7/2}}=0.13 .$$

The values of the rotation angles θ for the initial Rydberg states are given in Table II and plots of the fit and the data for several typical scans are shown in Fig. 6. Levels with $n>19$ were not used to fit the parameters due to the noise level of the data. We note that the parameters we list here are the set of energy-independent parameters which best fit all the data above the $6p_{1/2}$ limit simultaneously. Often the value of χ^2 for the fit of a given n level could be reduced by over a factor of 3 by changing the values of one or two of the MQDT parameters by up to

TABLE II. Rotation angle θ which describes the relative amplitudes of the jj coupled $6snf$ states in the actual $6snf$ doublets. Values listed were obtained by determining the best fit for the $6p_{3/2}nf$ data above the $6p_{1/2}$ limit. Also shown is the member of the doublet for a given n which was previously assigned as the singlet level (see Ref. 9). Note that in the representation scheme used here, a doublet with a red state, which is pure singlet, has a rotation angle value of $\theta=0.2728\pi$ while a doublet with a blue singlet state has $\theta=0.7728\pi$.

n	θ	Previous singlet classification
7	0.744π	blue
8	0.826π	blue
9	0.273π	red
10	0.327π	blue
11	0.157π	blue
12	0.126π	blue
13	0.209π	red
14	0.210π	red
15	0.788π	red
16	0.896π	red
17	0.292π	red
18	0.678π	blue
19	0.660π	blue

15%. However, the value of the MQDT fit stems from the energy independence of the parameters, and although fitting the levels independently can produce asthetically pleasing results, the physical insight gained is minimal.

In Fig. 6 the profiles are labeled according to the value of the principal quantum number n of the initial Rydberg state. The amplitude of each labeled profile was normalized to 1 individually. States labeled as (i) were excited from red initial states whereas those identified as (ii) originated from blue levels.

Six-channel analysis below the $6p_{1/2}$ limit

The six-channel fit was performed in much the same way as the four-channel fit with the obvious complication of another bound channel [ψ_3 of Eq. (2)] and another generalized continuum channel. To simplify the fitting procedure the parameters obtained from the four-channel fit were kept fixed when finding the best values for the new parameters. This method is correct since the values for all parameters above the limit are directly related to those below the limit. Only the bound-continuum and continuum-continuum interaction parameters need to be modified since the generalized continua of the four-

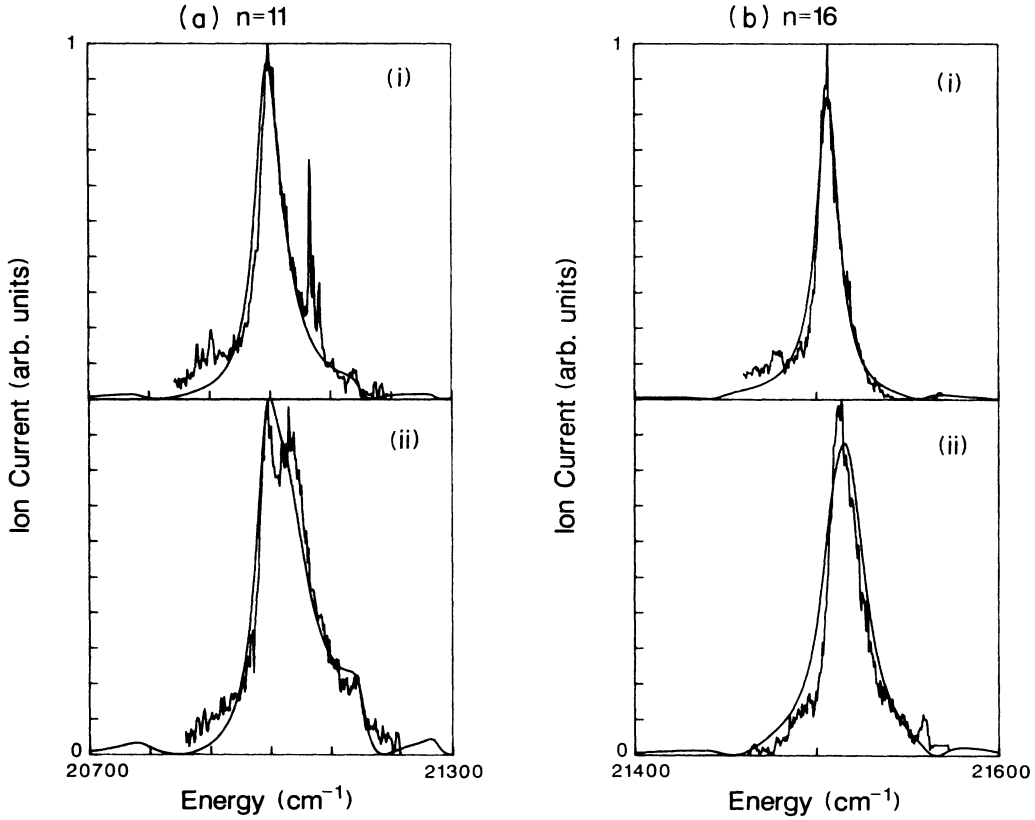

FIG. 6. Experimental excitation profiles of several members of the $6p_{3/2}nf\ J=4$ autoionizing series above the $6p_{1/2}$ limit for (a) $n=11$ and (b) $n=16$. Also included in the plots are the results of the four channel MQDT fit to the data (i) shows a data acquired from an initial red Rydberg state and (ii) an initial blue level. Each labeled feature in a given plot was obtained from a different initial level and individually normalized to 1. The energy scale is relative to the first ionization limit. Note that, in general, the profiles for a given n have completely different shapes for red and blue initial states due to the different amplitudes of the jj coupled basis states in the wave functions of these initial states. Another point of interest is the strong excitation of the $6p_{3/2}15p$ and $6p_{3/2}16p$ states in the excitation of the $6p_{3/2}11f$ (red) level.

channel fit are not the same as those in the six-channel case. Above the $6p_{1/2}$ limit bound channel 3 becomes a continuum channel, thus the total projection of the bound channels on the continua above the limit is the same as their projection onto the continua and bound channel 3 below the limit. The length of the projection must be a constant above and below the limit. Therefore we have

$$|R^+_{13}|=[(R'_{13})^2+(R'_{14})^2]^{1/2}$$

and

$$|R^+_{25}|=[(R'_{23})^2+(R'_{25})^2]^{1/2},$$

where the R^+ correspond to the R' matrix elements obtained from the four-channel model above the $6p_{1/2}$ limit. Above the $6p_{1/2}$ limit this has the obvious interpretation that the autoionization rates must be the same irrespective of whether a four- or six-channel model is used.

Once again the amplitude of the calculated cross section was left arbitrary for any given scan and the angular ratios used for the bound channels are $\chi_2/\chi_1=\sqrt{5/12}$ and $\chi_3/\chi_1=-\sqrt{7/12}$. The values for the MQDT parameters which best fit the observed data are

$$\underline{R'}=\begin{bmatrix} 0 & -0.083 & -0.25 & 0.59 & 0 & 0 \\ -0.083 & 0 & -0.35 & 0 & 0.71 & 0 \\ -0.25 & -0.35 & 0 & 0 & 0 & 0.87 \\ 0.59 & 0 & 0 & 0 & -0.050 & -0.76 \\ 0 & 0.71 & 0 & -0.050 & 0 & -0.22 \\ 0 & 0 & 0.87 & -0.76 & -0.22 & 0 \end{bmatrix},$$

$$\delta_1=\delta_{6p_{3/2}nf_{5/2}}=0.31,$$

$$\delta_2=\delta_{6p_{3/2}nf_{7/2}}=0.13,$$

and

$$\delta_3=\delta_{6p_{1/2}nf_{7/2}}=0.20.$$

Plots of the data and the six-channel fit for several states are shown in Fig. 7. Unfortunately, in this case the fine details of every excitation cannot be reproduced by a single set of energy-independent parameters. In particular, the structure in the $6p_{3/2}7f$ and $6p_{3/2}8f$ levels is not well reproduced using the MQDT parameters listed above. Although we can reproduce the spectra of these perturbed states reasonably well using modified sets of parameters, the value of such a fit is minimal. Possible reasons for the discrepancies in the data and the theoretical fits will be discussed briefly in the next section.

Validity of the theoretical method

We believe that the major problems with our theoretical model stem from two main sources. The first is the small number of bound channels which we have allowed in our theoretical description. We have only considered excitations to the three most probable $6p_jnf_{j'}$ $J=4$ levels. In doing so we have neglected seven other $6pnf$ $J=2,3$ configurations which make up nearly 10% of the total excitation to $6pnf$ levels. Furthermore, we have completely ignored other possible configurations such as $6pnp$ and $6dnd(s)$. In fact, in frequency scans showing the excitation of the $6p11f$ levels, there are clearly additional sharp features in the profile due to excitation of $6p15p$ and $6p16p$ levels. These added features are particularly noticeable for the broad levels we have observed since the cross sections are nonzero for the entire frequency range between the $n-1$ and $n+1$ nodes in the overlap integral. Thus we are forced to study the entire energy range and not just small frequency intervals near narrow levels.

Also, it should be noted that the ICE technique itself may prove to be more of a hindrance than a help for such short-lived states. For long-lived energy levels, the spectral densities $|A_i|^2$ usually determine the major features of the excitation spectrum with only a slight modulation due to the overlap integral of the spectator electron. Under these circumstances fitting MQDT parameters to the data is a reasonable (although perhaps a tedious) task. In contrast, for states whose widths are of the same order as the spacing between adjacent energy levels, the overlap integral becomes the dominant feature of the profile. Fitting MQDT parameters to the spectra in these cases is far more difficult since the basic features of the observed cross section can be extremely independent of channel mixings and even the energy-level positions. Therefore finding the correct parameters to describe the system verges on the impossible since there are many shallow minima in the parameter space, and all of these minima can fit the data to nearly the same degree.

In order to illustrate the point consider the $6p_{1/2}nf$ excitation data shown in Fig. 8(a). The smooth curve shown with the data is simply the overlap integral of Eq.

(5) with no contribution from the spectral amplitude $A(\nu)$. Examination of the figure clearly shows that the shape of the feature is dominated by the overlap integral whose shape only depends on the energy of the initial $6snf$ Rydberg state. By examining the amplitude of the data in relation to the overlap integral in the wings of the main feature, it is clear that the spectral density $|A(\nu)|^2$ never has a value less than 25% of its maximum over the energy range of interest. This point is clearly exhibited in Fig. 8(b) where we have plotted the spectral density $|A_3|^2$ over the same energy range shown in Fig. 8(a). Thus the spectral amplitude A_3 does not have the familiar structure of a series of peaks with near zeros between them, but instead, consists of a high background (approximately 50% of maximum) topped by a broad oscillation. In any case the parameters of the $6pnf$ autoionizing series are not easily derived from these spectra, which are dominated by the characteristics of the $6snf$ series.

Figure 9 serves to show the difficulty we encountered when trying to assign quantum defects and decay rates to the observed data. In Fig. 9 we show calculated spectra of excitation to the $6p_{3/2}11f_j$ autoionizing states. The calculation uses the four-channel approach discussed above with the best fit parameters obtained for that fit. The only parameters that are allowed to vary in the four figures are the bound-continuum interaction parameters, but the ratio of these two pseudowidths is kept constant. Previous MQDT treatments have dealt with states whose widths were comparable to those shown in Fig. 9(a). The widths of the states we report here are slightly greater than those corresponding to Fig. 9(c). Therefore, it is not surprising that we have found several sets of parameters that reproduce the data with nearly the same accuracy. Examination of these figures clearly shows the relative ease in determining the positions and FWHM's of the states in Figs. 9(a) and even 9(b) compared to Figs. 9(c) and 9(d).

V. REVIEW OF Ba $6pnl$ AUTOIONIZATION RATES

Over the last ten years many extensive studies of Ba autoionizing levels have been performed. In particular, the energy-level positions and autoionization rates of many $6pnl$ states have been determined. In fact, with the data from this work, the scaled decay rates $n^3\Gamma$, and the quantum defects have been measured for values of $l<11$ for the $6p_{1/2}nl$ states and for $l<5$ for the $6p_{3/2}nl$ levels.

The total decay rate of an autoionizing level may be written as

$$\Gamma=\Gamma_{\text{spontaneous}}+\Gamma_{\text{autoionization}}\ .$$

In Fig. 10 we show a plot of the scaled total decay rates $n^3\Gamma$ as a function of l for $6p_{1/2}nl\,J=l+1$ levels. The de-

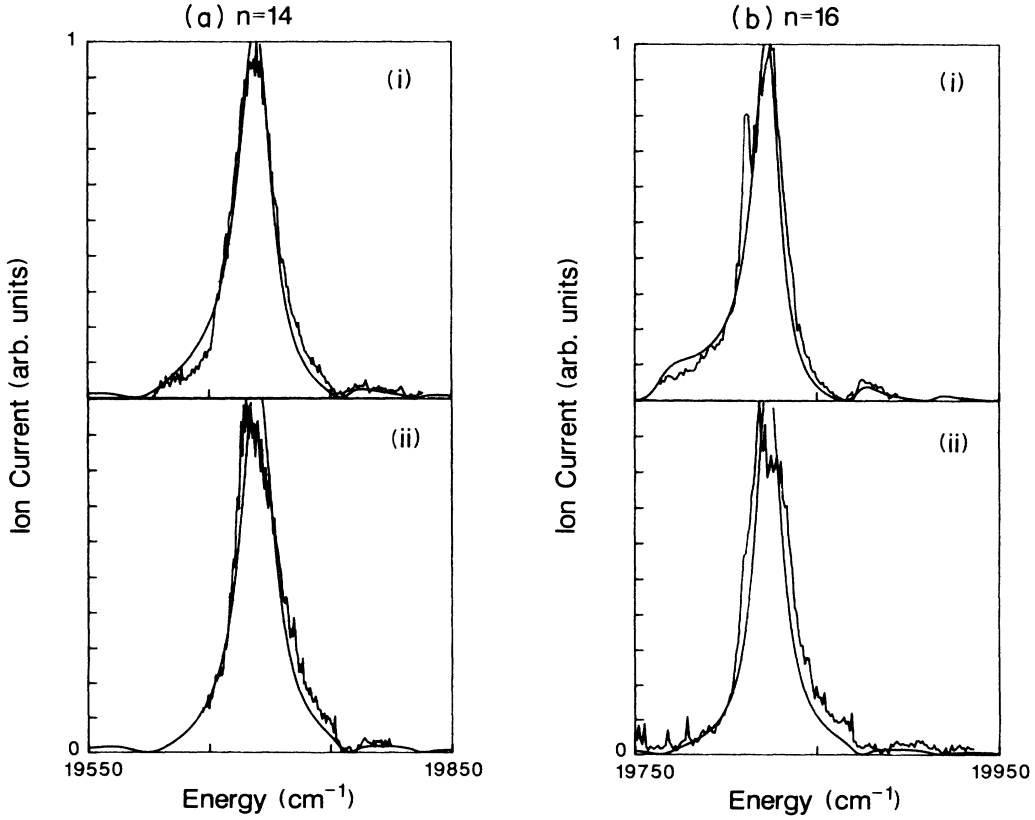

FIG. 7. Excitation profiles of several members of the $6p_{1/2}nf_{7/2}$ $J=4$ series for (a) $n=14$ and (b) $n=16$, completely analogous to Fig. 6. The fit to the data is the result of calculations based on the six-channel MQDT model.

cay rates shown are given in atomic units and are the average rates over many n states for $l=0$–4. For $l>4$ the experimental rates plotted correspond to those measured for $n=12$.[12] It is necessary to choose a particular n value for the higher l states due to the fact that the rates only scale strictly as n^3 for $n \gg l$. Note the constant decay rate for the highest l states which corresponds to the spontaneous decay rate of the Ba^+ $6p_{1/2}$ level of 26 MHz.[13] The solid line is a theoretical calculation which models the autoionization process as a dipole interaction between a hydrogenic Rydberg electron and a Coulomb core electron.[12] The model works quite well for the high-l levels, but obviously breaks down for the low angular momentum states which are nonhydrogenic and have a significant core penetration. One interesting feature of Fig. 10 is that the core penetration of the

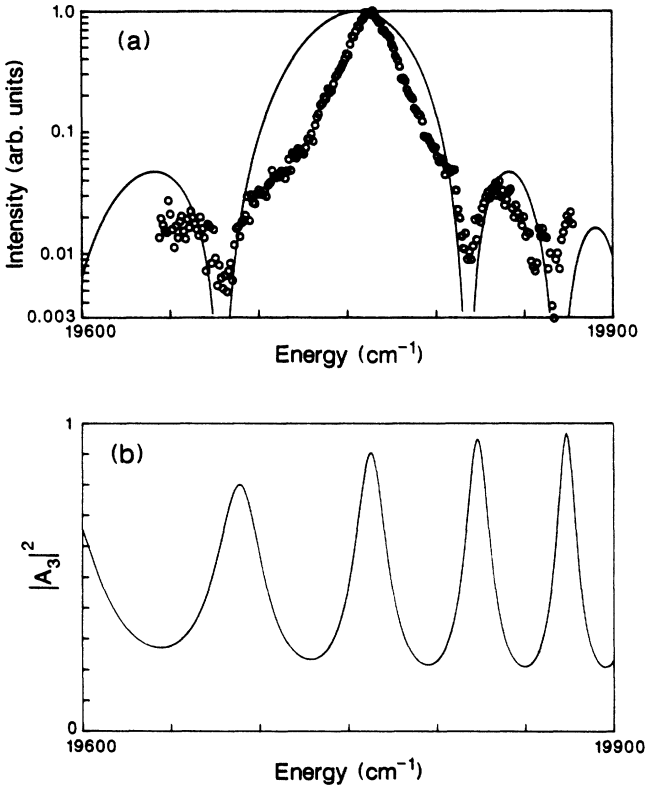

FIG. 8. Experimental cross section for excitation of the $6p_{1/2}15f_{7/2}$ $J=4$ level plotted vs energy. Also shown is the overlap integral from the initial to the final Rydberg state. The figure clearly shows that the shape of the excitation profile is dominated by the overlap integral and not by the final-state spectral density. Thus the final excitation cross section is dominated by the energy of the initial state only with little dependence on the character of the final state. The energy scale is relative to the first ionization limit. (b) Calculated spectral density $|A_3|^2$ for excitation of the autoionizing channel labeled $6p_{1/2}nf_{7/2}$ plotted vs energy. Note the large background between adjacent maxima due to the overlapping tails of the broad resonances. The decrease in the amplitude at the low-energy end of the scale is due to mixing of the $6p_{1/2}$ channel with the $6p_{3/2}7f_j$ levels. The energy scale is relative to the first ionization limit.

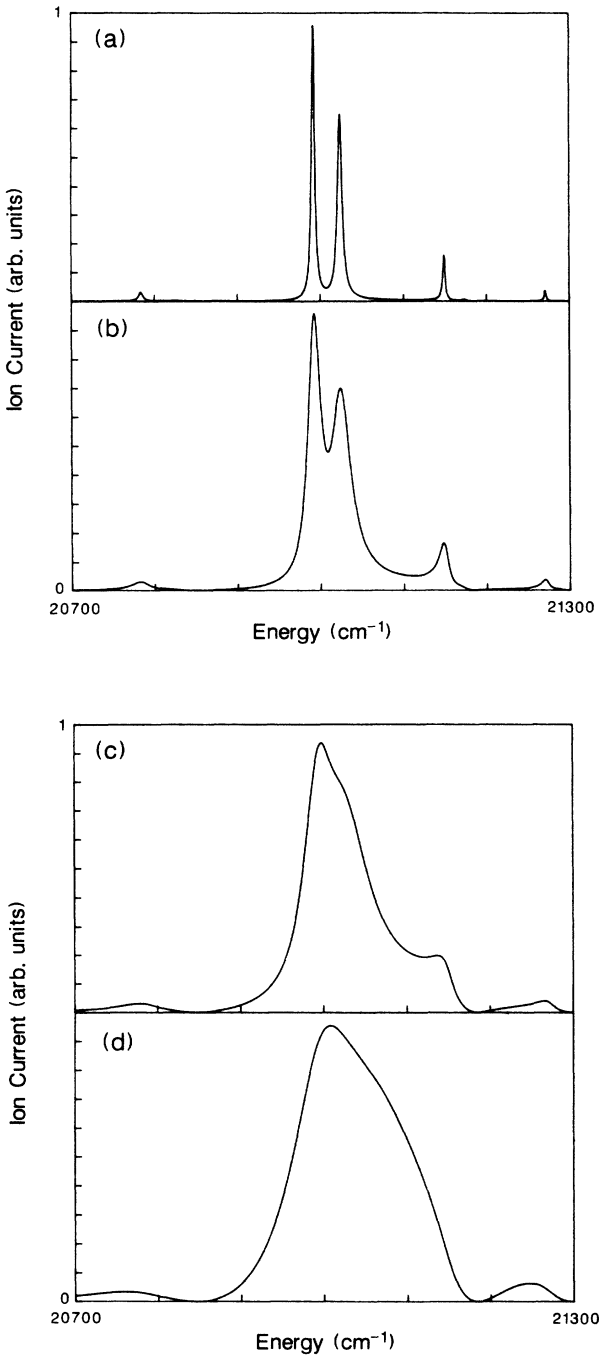

FIG. 9. Calculated cross section for excitation of the $6p_{3/2}11f_j$ states from an initial $6s_{1/2}nf$ blue level. The calculation is based on our four-channel MQDT model. The parameters used for the calculation are identical to those given in the text with the exception of the bound-continuum interactions R'_{13} and R'_{24}. The values of the parameters shown are (a) $R'_{13}=0.20$, $R'_{24}=0.25$; (b) $R'_{13}=0.40$, $R'_{24}=0.50$; (c) $R'_{13}=0.60$, $R'_{24}=0.75$; (d) $R'_{13}=0.80$, $R'_{24}=1.0$. Note that in (a) the peak positions and FWHM are readily obtainable for both fine-structure components. In (c) and (d) the fine-structure components are overlapped and the final-state parameters are not easily derived from the raw spectra. The parameters obtained from our four-channel fit are $R'_{13}=0.63$ and $R'_{24}=0.80$ which describe a set of states slightly broader than those shown in (c).

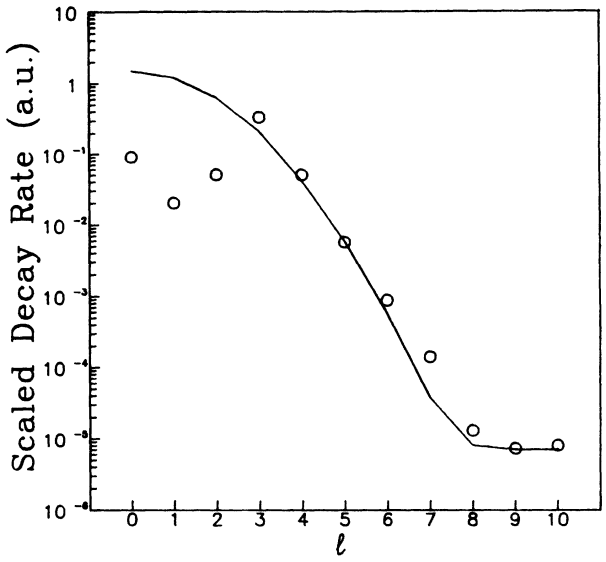

FIG. 10 Plot of scaled total decay rates $n^3\Gamma$ of Ba $6p_{1/2}nl$ $J=l+1$ autoionizing states in atomic units vs l. For $l=0$–4 the measured rates (○) shown are the average rates from measured data ($l=0,1,2,4$, see Refs. 14, 15, 2, and 4, respectively). Since the n^{-3} scaling is an approximation valid for $n \gg l$ only, the data for the rates for $l>4$ are for a particular n value ($n=12$, see Ref. 12). The solid line is a simple theoretical calculation based on the dipole scattering of a hydrogenic Rydberg electron from the $6p$ core electron. Note that the core penetration of the lower-l states reduces the rate from the dipole scattering model. The constant total decay rate for $l>8$ is the spontaneous decay rate of the Ba^+ $6p$ state at 25.5 MHz.

lowest angular momentum states $l<3$ lowers the autoionization rates. One might think that a deep core penetration should increase the possibility of scattering between the two electrons, but apparently, an interaction at a small radius strongly damps any scattering process.

The other obvious feature in Fig. 10 is the strong peak in the autoionization rates for the f states. The f electrons obviously spend a relatively large fraction of their orbit near enough to the core electron that there is a large scattering probability while still having only minimal exchange interaction with the other electron. We believe that the explanation of this effect lies in the fact that the f electrons never significantly enter the Ba^{2+} core while the lower angular momentum electrons do. This fact is clear after examination of the Ba $6snl$ and Ba^+ nl quantum defects. For both neutral and singly charged barium Rydberg states, the quantum defects for the $l<3$ states are greater than 2.3. These large quantum defects are due predominantly to core penetration effects. The quantum defects for the higher-l states are significantly lower and can be reproduced reasonably well using a core polarization model (with no core penetration).

Figure 10 clearly shows that the observed decay rates follow the independent hydrogenic particle model extremely well for $l>2$. Thus, as alluded to above, it seems that the core penetration of the lower-l states causes the substantial reduction in the observed autoionization rates. A possible classical mechanism for this reduction is the fact that once inside the Ba^{2+} core, there can be no energy exchange between the outer-shell electrons. Thus it seems that much of the time that the low-l Rydberg electron is within scattering range of the other valence electron, one of the two is imbedded in the Ba^{2+} electron cloud where scattering is prohibited.

VI. CONCLUSION

We have measured the autoionization rates and energy-level positions of Ba $6p_j nf_{j'}$ states for $n=7$–30. The experimental widths of the ICE spectra are comparable to the spacings between adjacent energy levels. We have also performed a MQDT analysis of the data and have reported the results of the parameter fit. The results of our analysis reproduce the observed spectra reasonably well considering the number of approximations made. The use of the isolated core model on these extremely short-lived states may be questionable, but the fact that the data have been reproduced fairly well suggests that the model may be useful even outside of its region of strict validity.

ACKNOWLEDGMENTS

It is a pleasure to acknowledge useful discussions with W. E. Cooke. This work has been supported by the U.S. Department of Energy, Office of Basic Energy Sciences, Chemical Sciences Division.

[1]W. E. Cooke, T. F. Gallagher, S. A. Edelstein, and R. M. Hill, Phys. Rev. Lett. **40**, 178 (1978).
[2]F. Gounand, T. F. Gallagher, W. Sander, K. A. Safinya, and R. Kachru, Phys. Rev. A **27**, 1925 (1983).
[3]N. H. Tran, P. Pillet, R. Kachru, and T. F. Gallagher, Phys. Rev. A **29**, 2640 (1984).
[4]S. M. Jaffe, R. Kachru, H. B. van Linden van den Heuvell, and T. F. Gallagher, Phys. Rev. A **32**, 1480 (1985).
[5]Emily Y. Xu, Yifu Zhu, Oliver C. Mullins, and T. F. Gallagher, Phys. Rev. A **33**, 2401 (1986).
[6]T. W. Hansch, Appl. Opt. **11**, 895 (1972).
[7]W. E. Cooke, S. A. Bhatti, and C. L. Cromer, Opt. Lett. **7**, 69 (1982).
[8]C. E. Moore, *Atomic Energy Levels*, Natl. Bur. Stand. (U.S.) Circ. No. 467 (U.S. GPO, Washington, D.C., 1949), Vol. 3.
[9]B. H. Post, W. Vassen, W. Hogervost, M. Aymar, and O. Robaux, J. Phys. B **18**, 187 (1985).
[10]W. E. Cooke and C. L. Cromer, Phys. Rev. A **32**, 2725 (1985).
[11]S. A. Bhatti, C. L. Cromer, and W. E. Cooke, Phys. Rev. A **24**, 161 (1981).
[12]R. R. Jones and T. F. Gallagher, Phys. Rev. A **38**, 2846 (1988).
[13]A. Lindgard and S. E. Nielsen, At. Data Nucl. Data Tables **19**, 613 (1977).
[14]W. E. Cooke (private communication).
[15]E. A. J. M. Bente, Ph.D. thesis, Vrije University, Amsterdam, 1989.